Geophysical Journal International

Geophys. J. Int. (2016) **206,** 630–643
Advance Access publication 2016 April 22
GJI Seismology

doi: 10.1093/gji/ggw161

Earthquake rate and magnitude distributions of great earthquakes for use in global forecasts

Yan Y. Kagan and David D. Jackson

Department of Earth, Planetary, and Space Sciences (EPSS), Geology Bldg, 595 *Charles E. Young Dr., University of California, Los Angeles (UCLA), Los Angeles, CA* 90095-1567, *USA. E-mail: ykagan@ucla.edu*

Accepted 2016 April 20. Received 2016 April 19; in original form 2015 November 26

SUMMARY

We have obtained new results in the statistical analysis of global earthquake catalogues with special attention to the largest earthquakes, and we examined the statistical behaviour of earthquake rate variations. These results can serve as an input for updating our recent earthquake forecast, known as the 'Global Earthquake Activity Rate 1' model (GEAR1), which is based on past earthquakes and geodetic strain rates. The GEAR1 forecast is expressed as the rate density of all earthquakes above magnitude 5.8 within 70 km of sea level everywhere on earth at 0.1 × 0.1 degree resolution, and it is currently being tested by the Collaboratory for Study of Earthquake Predictability. The seismic component of the present model is based on a smoothed version of the Global Centroid Moment Tensor (GCMT) catalogue from 1977 through 2013. The tectonic component is based on the Global Strain Rate Map, a 'General Earthquake Model' (GEM) product. The forecast was optimized to fit the GCMT data from 2005 through 2012, but it also fit well the earthquake locations from 1918 to 1976 reported in the International Seismological Centre-Global Earthquake Model (ISC-GEM) global catalogue of instrumental and pre-instrumental magnitude determinations. We have improved the recent forecast by optimizing the treatment of larger magnitudes and including a longer duration (1918–2011) ISC-GEM catalogue of large earthquakes to estimate smoothed seismicity. We revised our estimates of upper magnitude limits, described as corner magnitudes, based on the massive earthquakes since 2004 and the seismic moment conservation principle. The new corner magnitude estimates are somewhat larger than but consistent with our previous estimates. For major subduction zones we find the best estimates of corner magnitude to be in the range 8.9 to 9.6 and consistent with a uniform average of 9.35. Statistical estimates tend to grow with time as larger earthquakes occur. However, by using the moment conservation principle that equates the seismic moment rate with the tectonic moment rate inferred from geodesy and geology, we obtain a consistent estimate of the corner moment largely independent of seismic history. These evaluations confirm the above-mentioned corner magnitude value. The new estimates of corner magnitudes are important both for the forecast part based on seismicity as well as the part based on geodetic strain rates. We examine rate variations as expressed by annual earthquake numbers. Earthquakes larger than magnitude 6.5 obey the Poisson distribution. For smaller events the negative-binomial distribution fits much better because it allows for earthquake clustering.

Key words: Probability distributions; Seismicity and tectonics; Statistical seismology; Subduction zone processes; Dynamics: seismotectonics.

1 INTRODUCTION

For nearly two decades we have constructed testable global earthquake forecasts using spatial, temporal and magnitude distributions of earthquakes in the Global Central Moment Tensor (GCMT) catalogue (Ekström *et al.* 2012). Our models employ 'smoothed seismicity', in which the earthquake 'rate density' (earthquakes per unit area, magnitude and time) is specified on a global grid. The models assume a modified Gutenberg–Richter ('MGR' or 'TGR') magnitude distribution with three parameters: the rate of events at a lower magnitude threshold, the 'b-value' and a 'corner magnitude' at which the earthquake rate fall below that assumed in the basic

2-parameter G-R model (Kagan 2002a). We have used two alternative representations, the 'Gamma' and the tapered Gutenberg-Richter ('TGR'), each of which has its own corner magnitude parameter. Neither of the modified G-R distributions has a firm theoretical basis; both were devised to assure that the implied seismic moment rate is finite, which is not true for the classical 2-parameter G-R distribution. Fitted to the same earthquake catalogue, the two distributions have slightly different corner magnitudes, although they predict nearly identical rates as a function of magnitude. Thus the choice between them is somewhat arbitrary at present, but future investigation with more great earthquakes may favour one over the other. Studies using just catalogues with copious data generally show a clear maximum likelihood estimate for the corner magnitude, although the 95 per cent confidence limit is open to infinity, implying that the 2-parameter G-R model is not rejected by the catalogue alone. We have found, however, that the 'tectonic moment' deduced from surface deformation data does impose a useful upper magnitude limit (Kagan 2002b). Our goal in this paper is to investigate that upper limit, and the estimated rate at the lower magnitude threshold, for the most recent global earthquake data, which contain important great earthquakes not fully incorporated in previous forecasts.

Our most recent application has been the 2015 GEAR1 forecast (Bird *et al.* 2015), which combines a smoothed seismicity and tectonic deformation inferred from geological and geodetic information. In the tectonic component we used earthquake data indirectly to describe a small number of tectonic zone types. Here we use newly available earthquake data and the moment-rate balance principle to re-evaluate threshold rates, the *b*-values and corner magnitudes assumed in the forecasts. The new data include recent giant earthquakes as well as catalogued events over the last century recently made available by the Global Earthquake Model (GEM) project. The new results agree with previous estimates within their errors, indicating that the forecast models are robust with respect to catalogue additions. The corner magnitude estimates have increased modestly in response to the recent huge events. As before, we find that the *b*-values are statistically indistinguishable among spreading ridges, continental margins and subduction zones, while *b*-values for fast and slow spreading ridges may be higher than for other tectonic regions. The global rate of magnitude 9 earthquakes is about 3 per century whether we assume the Gamma or the TGR magnitude distribution.

Scientists from academia, government, the private sector and the Collaboratory for Study of Earthquake Predictability (CSEP) have been constructing and testing a global earthquake rate model as a function of magnitude at 0.1 by 0.1 degree resolution (Bird *et al.* 2015). Nicknamed 'GEAR1', the model relies on a global strain rate model (GSRM) and instrumental earthquake catalogues. After testing, the model can be used by the GEM and others in seismic hazard estimation. GEAR1 covers the magnitudes 5.8 and larger and time intervals from years to decades with no explicit time-dependence.

In GEAR1 the seismic and strain-rate components of the model are specified separately and then combined optimally to fit earthquake occurrence over the last several years. GEAR1 performs well in quasi-prospective tests using the GCMT catalogue (Ekström *et al.* 2012) after 2005 and the International Seismological Centre-Global Earthquake Model (ISC-GEM) catalogue (Storchak *et al.* 2015) from 1918 to 1976; GEAR1 will be tested prospectively against future earthquakes. In GEAR1 model, the forecast is based on the magnitude distribution results obtained by Kagan *et al.* (2010), that is, on the seismicity data up to 2008 March 31.

Though GEAR1 qualitatively takes into account later seismicity record, we perform a more rigorous quantitative statistical analysis of these data. Here we revise our estimates of the upper magnitude limits, based on the massive earthquakes since 2004 and the seismic moment conservation principle. The new estimates of the corner magnitudes are important both for the forecast part based on seismicity as well as the part based on geodetic strain rates, where the corner magnitudes are used for the rates calibration. These new estimates will be used in the new revised version of the GEAR1 model.

In this work, we update the magnitude/frequency distribution (Section 3) based on additional data from the GCMT, Preliminary Determinations of Epicenter (PDE) and ISC-GEM catalogues (see Section 2), and institute a forecast test of earthquake numbers (Schorlemmer & Gerstenberger 2007; Zechar *et al.* 2013) based on the negative-binomial distribution (NBD) (Section 4).

2 CATALOGUES

We studied earthquake distributions and clustering for the global CMT (Centroid-Moment-Tensor) catalogue of moment tensor inversions compiled by the GCMT group (Ekström *et al.*, 2012, and references therein). The present catalogue contains close to 43 000 earthquake entries for the period 1977/1/1 to 2014/12/31. The event size is characterized by a scalar seismic moment M. The completeness threshold is about $m5.8$ for the full catalogue, and $m5.6$ starting with 1982 (Kagan 2003).

We also experiment with a forecast based on the U.S. Geological Survey (2008) PDE catalogue. The PDE catalogue has substantial advantages over the GCMT one. The PDE has a longer observation period (the surface wave magnitude m_S was determined starting from the middle of 1968), and a lower magnitude threshold (m_t). Depending on the time period and the region, the threshold is of the order 4.5 to 4.7 (Kagan 2003), that is, much lower than the GCMT catalogue threshold (around 5.4 to 5.8). As a precaution in our analysis of the PDE catalogue we used the threshold $m_t = 5.0$.

Storchak *et al.* (2015) released the ISC-GEM catalogue, which is a comprehensive revision of the longstanding ISC catalogue. This new catalogue is believed to be relatively complete for the threshold $m_t = 6.5$ (Di Giacomo *et al.* 2015) or $m_t = 7.0$ (Michael 2014) from 1918 to 2011. In those years which predate the routine production of the GCMT solutions, there were 881 shallow earthquakes of $m6.8+$.

We define geographically contiguous areas of the related tectonic style, and define the union of all areas with the same style as a 'tectonic zone' (see Fig. 1). The algorithm and data sets defining these zones were presented by Bird (2003) and Kagan *et al.* (2010). Similarly, slightly modified zones are used in the GEAR1 project (Bird & Kreemer 2015, fig. 2) for constructing tectonic forecast. Since the GEAR1 seismic forecast was based on 2010 zones, we use them in our work.

3 FREQUENCY-MOMENT RELATION

Here we analysed statistically the distribution of seismic scalar moment for earthquakes in different tectonic environments and temporal periods. We use the scalar seismic moment M directly, but for an easy comparison and display we convert it into an approximate moment magnitude using the relationship (Hanks 1992)

$$m_W = \frac{2}{3}(\log_{10} M - C), \quad (1)$$

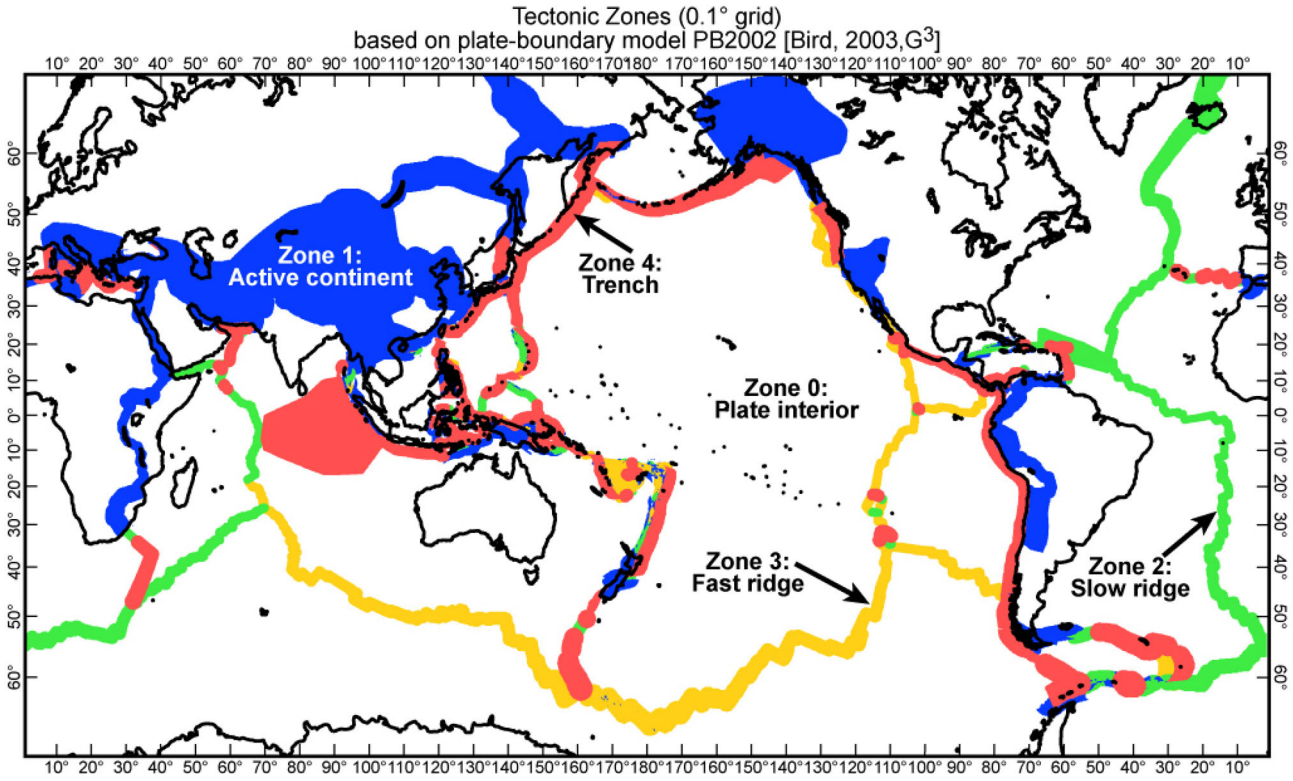

Figure 1. Global tectonic zones.

where $C = 9.0$, if moment M is measured in Newton m (N m), and $C = 16.0$ for moment M expressed in 'dyne cm' as in the GCMT catalogue. The equation above provides a unique mapping from magnitude to moment, so, where appropriate, we will use the same subscripts for both M and m. Thus $m_{\max}$ implies a corresponding $M_{\max}$, etc.

3.1 Method

3.1.1 Theoretical distributions

In this work we consider two statistical distributions of the scalar seismic moment (Kagan 2002a): (1) the TGR or equivalently tapered Pareto distribution, in which the upper magnitude parameter is the corner magnitude, $m_{\rm cm}$, and (2) the Gamma distribution, in which the upper magnitude parameter is the corner magnitude $m_{\rm cg}$.

The corner moment and the asymptotic spectral slope (β) are the two parameters of the TGR model for the complementary cumulative density function of seismic moments (herein called the 'moment distribution'). In this form the distribution is more familiar to seismologists:

$$G\,(M,\,M_t,\,\beta,\,M_{\rm cm}) \;=\; (M_t/M)^{\beta}\,\exp\,[\,(M_t - M)/M_{\rm cm}\,] \quad \text{for} \quad M_t \le M \le \infty\,, \tag{2}$$

where G is the fraction of earthquakes (by event count) in the catalogue with the moment exceeding M, $M_{\rm cm}$ is the corner moment parameter controlling the distribution in the upper ranges of M, and M_t is lower threshold moment for the completeness of the catalogue (Kagan 2003). The β-value can be converted to b of the G-R law as $b = 1.5 \times \beta$. A similar distribution, called 'tempered' Pareto distribution, is often used in statistical literature, see for example, Meerschaert *et al.* (2012, eqs 2.1 and 2.2).

The Gamma distribution has the probability density function

$$\phi(M) \;=\; C^{-1}\,\frac{\beta}{M}\,(M_t/M)^{\beta}\,\exp[(M_t - M)/M_{\rm cg}], \quad \text{for} \quad M_t \le M < \infty, \tag{3}$$

where $M_{\rm cg}$ is the corner moment similar to that of eq. (2), and C is a normalizing coefficient. Specifically,

$$C \;=\; 1 \;-\; (M_t/M_{\rm cg})^{\beta}\,\exp(M_t/M_{\rm cg}) \times \Gamma(1-\beta,\,M_t/M_{\rm cg})\,, \tag{4}$$

where Γ is the gamma function (Bateman & Erdelyi, 1953). For $M_{\rm cg} \gg M_t$ the coefficient $C \approx 1$.

Thus, each distribution is controlled by two parameters: its slope for small and moderate earthquakes, β, and its corner moment $M_{\rm cm}$ or $M_{\rm cg}$ that describes the behaviour of the largest earthquakes. The two equations above are normalized distributions. Both need a multiplicative constant and the threshold earthquake rate α_0 to calculate the rates at any magnitude above the threshold.

From the corresponding probability density functions we calculate (Kagan 2002b, eq. 7) the theoretical seismic moment release rate $\dot{M}_s$ (moment flux). For the TGR distribution the formula is

$$\dot{M}_s \;=\; \frac{\alpha_0\,M_0^{\beta}}{1-\beta}\,M_{\rm cm}^{1-\beta}\,\Gamma(2-\beta)\,\xi_m\,, \tag{5}$$

where ξ_t in this and the following formula is a correction coefficient necessary if m_0 magnitude is close to m_c, otherwise $\xi \to 1$. For the Gamma distribution the formula is

$$\dot{M}_s \;=\; \frac{\alpha_0\,M_0^{\beta}\,\beta}{1-\beta}\,M_{\rm cg}^{1-\beta}\,\Gamma(2-\beta)\,\xi_g\,. \tag{6}$$

Comparing seismic moment rate with tectonic moment rate we can evaluate the corner moment values $M_{\rm cm}$ and $M_{\rm cg}$ (see Section 3.3).

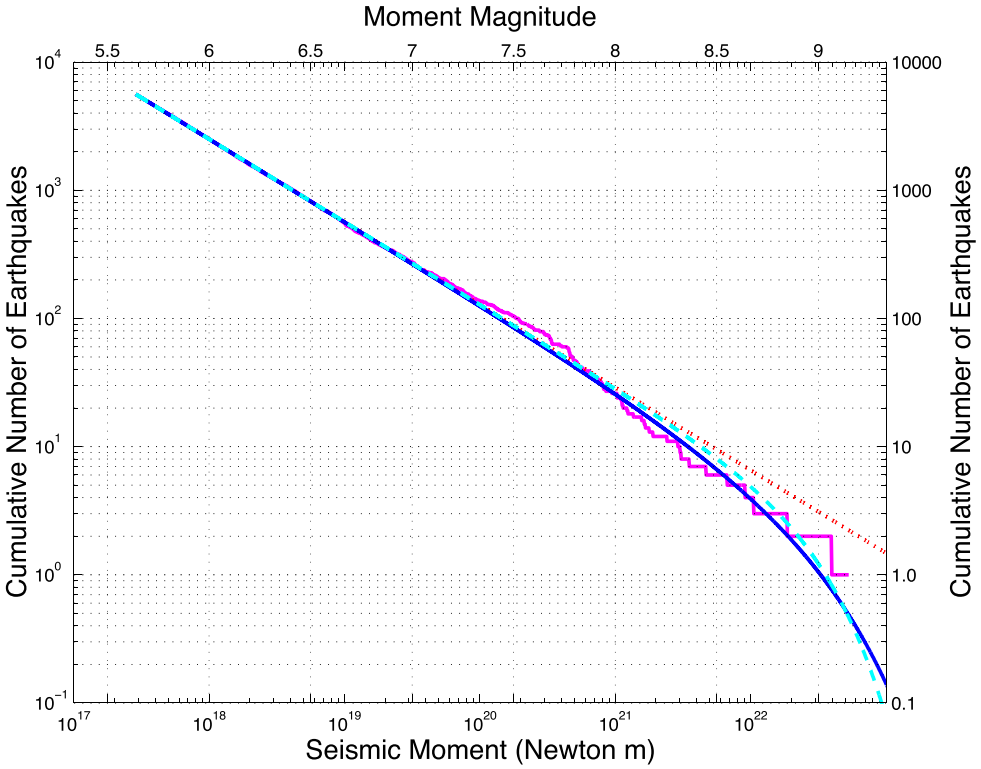

Figure 2. Number of earthquakes with moment (M) larger than or equal to M as a function of M for the shallow earthquakes in the CMT catalogue during 1982–2014, moment threshold $M_t = 10^{17.4}$ N m ($m_t = 5.6$), the total number of events 5607 (see Table 1). The empirical distribution is shown as the red step-function. Power-law approximation (equivalent to Gutenberg–Richter law) is shown by dotted line. Solid line shows tapered Gutenberg–Richter distribution: the G-R law restricted at large seismic moments by an exponential taper with the corner magnitude $m_{\rm cm} = 9.02$ (see eq. 2). Dashed line shows the Gamma distribution (eq. 3): the corner magnitude $m_{\rm cg} = 9.31$. The slope of the linear part of the curve corresponds to $\beta = 0.646$.

3.1.2 Statistical data analysis

Fig. 2 displays empirical cumulative distribution (survivor function) for the scalar seismic moment of trench shallow earthquakes (see Fig. 1) in the CMT catalogue for 1982–2014. The curves display a scale-invariant G-R (Pareto) distribution (linear in the log–log plot) which fits well small and moderate values of the moment magnitude m. But for large m, the empirical curve clearly bends downwards (see fig. 1 by Kagan 2002a for comparison). Approximations of the survivor function by the TGR and Gamma distributions are also shown. Both these theoretical distributions agree reasonably well with the observations, although the TGR curve fits better around $m \simeq 8.5$. Though in recent publications (Bird *et al.* 2015) we preferred the TGR law over the Gamma, additional investigations are needed.

In the GEAR1 model (Bird *et al.* 2015) as estimates of the corner magnitude and the β parameter we used mostly the results by Kagan *et al.* (2010) and by Bird & Kagan (2004). These estimates have been obtained by statistical analysis of the GCMT catalogue, using mostly 2-D (m_c versus β) likelihood maps. In this work we are using the GCMT catalogue updated until the end of 2014, as well as the GEM and the PDE catalogues (Section 2).

Kagan & Jackson (2013) argue that for global seismicity as well as for subduction zones the corner magnitude is likely to be as high as $m10$ with the suggested recurrence time of a few hundred or thousand years. Current results are consistent with this estimate. This means that the seismological data are insufficient to accurately estimate the upper magnitude limit. Therefore we apply several different statistical techniques to estimate the magnitude distribution parameters. If we obtain similar estimates of the parameters using significantly different methods, it would suggest that these approaches reveal the real values. Moreover, in addition to purely statistical analysis of seismic data we apply the moment conservation principle (Kagan 2002b) to evaluate the corner moment by comparing the tectonic and seismic moment rates (Section 3.3).

3.2 Evaluation of earthquake size distribution parameters by statistical analysis

We applied the likelihood method to obtain the estimates of β and m_c (Kagan 1997, 2002a). Fig. 3 displays the map of the log-likelihood function for two parameters of the TGR distribution. The β-value (around 0.61 ± 0.038) can be determined from the plot with sufficient accuracy, but the corner magnitude evaluation encounters serious difficulties. The upper contour of the 95 per cent confidence area in the likelihood map is not well-constrained and allows infinite $M_{\rm cm}$. This means that only the lower limit for $m_{\rm cm}$, around 8.7, can be reliably evaluated with the available data. Hence the maximum likelihood estimate ($m_{\rm cm} = 9.0$) is not well-constrained by the likelihood map. However, this $m_{\rm cm}$ value is significantly higher than the value measured for the GCMT catalogue with different time spans (Kagan 2002a, fig. 2; Kagan *et al.* 2010, table 1). This is because several very large earthquakes occurred recently.

Table 1 displays the values of the moment-frequency parameters for global tectonic zones (Fig. 1) that are estimated using various statistical techniques. This table is similar to table 4 by Kagan (2002a). Two time periods are selected—1982–2008

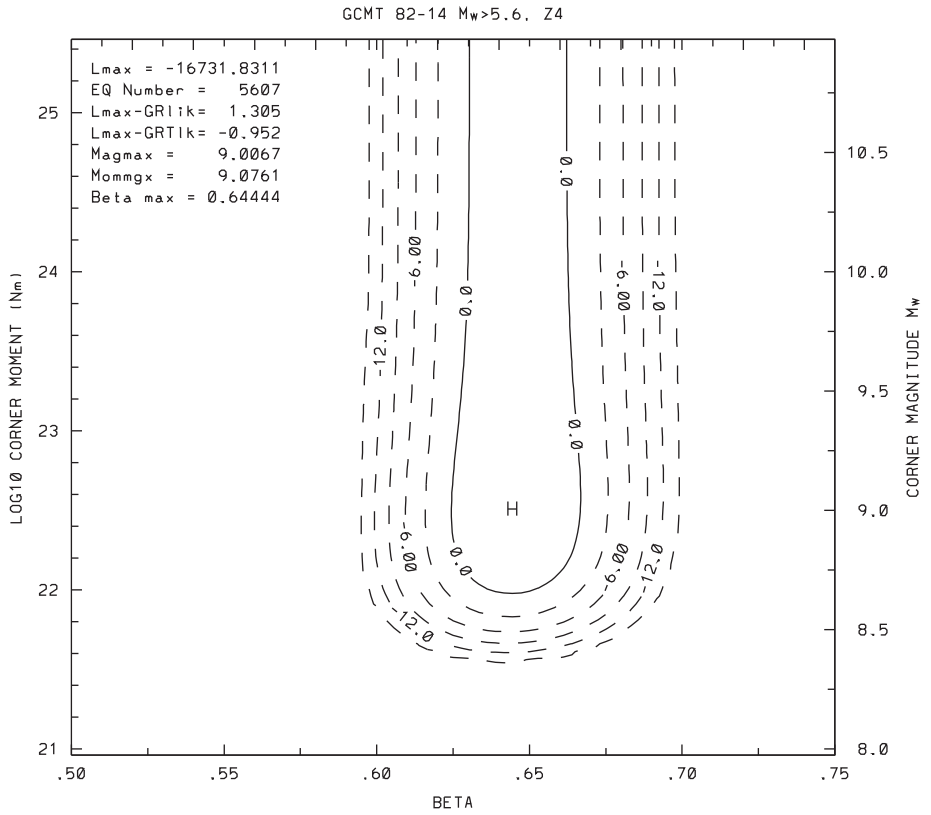

Figure 3. A log-likelihood map for the distribution of the scalar seismic moment of earthquakes in Trench tectonic zones (Fig. 1): the GCMT catalogue time span is 1982 January 1–2014 December 31; the seismic moment cut-off is $10^{17.4}$ N m ($m_t = 5.6$); the number of events is 5607. The approximation by the tapered G-R distribution (see eq. 2). The 'H' sign indicates the map maximum; the value of the function is adjusted to be 3.0 at this place. The zero contour (the solid line) corresponds to the 95 per cent confidence area (Kagan 1997).

Table 1. The β- and m_c-values in GCMT catalogue ($m_t = 5.6$) for tectonic zones (Fig. 1) specified by Kagan *et al.* (2010).

Tect. zone	n	$\hat{\beta} \pm \sigma_\beta$	$\tilde{\beta} \pm \sigma_\beta$	$\check{\beta} \pm \sigma_\beta$	$\hat{m}_{\rm cg} \pm \sigma_m$	$\hat{m}_{\rm cm} \pm \sigma_m$	$\tilde{m}_{\rm cm}$	$\check{m}_{\rm cm} \pm \sigma_m$	ρ
1	2	3	4	5	6	7	8	9	10
				1982–2008 March 31, $m_t = 5.6$					
Trench	4260	0.646 ± 0.010	0.644 ± 0.011	0.645 ± 0.010	9.05 ± 0.26	8.79 ± 0.23	8.88	8.80 ± 0.23	0.08
Act.cont.	867	0.665 ± 0.024	0.645 ± 0.024	0.651 ± 0.023	7.98 ± 0.19	7.68 ± 0.14	7.69	7.68 ± 0.14	0.23
Plate-int.	225	0.677 ± 0.045	0.669 ± 0.049	0.673 ± 0.045	8.58 ± 0.77	8.20 ± 0.45	8.10	8.21 ± 0.46	0.12
Slow-ridges	462	0.852 ± 0.040	0.842 ± 0.041	0.822 ± 0.042	6.96 ± 0.11	7.28 ± 0.15	7.07	7.25 ± 0.17	0.35
Fast-ridges	689	0.859 ± 0.033	0.850 ± 0.034	0.725 ± 0.041	5.82 ± 0.02	6.78 ± 0.07	6.68	6.64 ± 0.07	0.62
ALL	6503	0.680 ± 0.008	0.676 ± 0.009	0.679 ± 0.008	8.97 ± 0.23	8.78 ± 0.22	8.85	8.95 ± 0.31	0.06
				1982–2014, $m_t = 5.6$					
Trench	5607	0.646 ± 0.009	0.646 ± 0.010	$\sim \pm \sim$	9.31 ± 0.30	9.02 ± 0.24	9.01	$\sim \pm \sim$	$\sim$
Act.cont.	1109	0.657 ± 0.020	0.646 ± 0.022	0.646 ± 0.020	8.13 ± 0.19	7.81 ± 0.13	7.78	7.81 ± 0.13	0.20
Plate-int.	288	0.696 ± 0.041	0.687 ± 0.044	0.692 ± 0.041	8.50 ± 0.67	8.19 ± 0.44	8.08	8.19 ± 0.46	0.12
Slow-ridges	600	0.841 ± 0.034	0.831 ± 0.035	0.816 ± 0.036	7.16 ± 0.12	7.34 ± 0.15	7.15	7.32 ± 0.17	0.33
Fast-ridges	907	0.879 ± 0.029	0.870 ± 0.030	0.733 ± 0.037	5.29 ± 0.01	6.75 ± 0.06	6.64	6.60 ± 0.06	0.63
ALL	8511	0.680 ± 0.008	0.678 ± 0.008	0.669 ± 0.006	9.24 ± 0.28	9.02 ± 0.24	8.98	$\sim \pm \sim$	0.06

Notes: GCMT catalogue, see Ekström *et al.* (2012). n, the number of shallow (depth limit 0–70 km, $m \geq m_t$) events; $\hat{\beta}$ is estimated from a linear G-R fit over all magnitudes (eq. 22, all equation numbers here refer to Kagan 2002a), $\tilde{\beta}$ using a G-R fit for magnitudes ≤ 7.8 (eq. 24), and $\check{\beta}$ and its standard errors are calculated using a TGR fit that allows for a corner magnitude according to formulae in the Appendix (Kagan 2002a), same is done for $\check{m}_{\rm cm}$ in Column 9; $\hat{m}_{\rm cg}$ and its standard deviation are measured according to eqs (29), (30) and (34), assuming that β is known—taken from eq. (22); $\hat{m}_{\rm cm}$ and its standard deviation are measured according to eqs (31), (32) and (34), β is taken from eq. (24); $\tilde{m}_{\rm cm}$ is defined by eq. (35), that is, correcting for bias pointed by Kagan & Schoenberg (2001), $\beta = 2/3$ is assumed; ρ is calculated according to formula (A.22); $m_{\rm cg}$ and $m_{\rm cm}$ mean that the corner moment is defined according to the Gamma and TGR distribution, respectively. Sign '$\sim$' means that because of numerical problems in the iteration of IMSL procedure DRTMI, programs could not evaluate variables.

Table 2. Parameters of the tapered Gutenberg–Richter frequency/magnitude relations of the tectonic zones (Fig. 1) specified by Kagan *et al.* (2010), with 95 per cent confidence ranges.

		CMT82-08			CMT82-14			GEM18-11		
	Tectonic zone	n	β	$m_{\rm cm}$	n	β	$m_{\rm cm}$	n	β	$m_{\rm cm}$
4.	Trenches	4260	0.639	$8.75^{+\infty}_{-0.35}$	5607	0.646	$9.00^{+\infty}_{-0.35}$	1832	0.647	$8.53^{+\infty}_{-0.43}$
1.	Act.cont.	867	0.647	$7.59^{+0.72}_{-0.25}$	1109	0.646	$7.81^{+0.65}_{-0.25}$	522	0.711	$8.53^{+\infty}_{-0.75}$
0.	Plate-int.	225	0.639	$8.15^{+\infty}_{-0.53}$	288	0.690	$8.21^{+\infty}_{-0.60}$	111	0.702	$7.60^{+\infty}_{-0.45}$
2.	Slow-ridges	462	0.812	$7.38^{+\infty}_{-0.33}$	600	0.817	$7.34^{+\infty}_{-0.27}$	115	0.858	$6.93^{+\infty}_{-0.40}$
3.	Fast-ridges	689	0.767	$6.79^{+0.30}_{-0.18}$	907	0.737	$6.61^{+0.30}_{-0.18}$	80	0.990	$6.20^{+?}_{-?}$
	Global	6503	0.671	$8.73^{+\infty}_{-0.34}$	8511	0.678	$9.00^{+\infty}_{-0.37}$	2660	0.683	$9.47^{+\infty}_{-0.45}$

Notes: CMT82-08 is GCMT catalogue (Ekström *et al.* 2012) for time interval 1982–2008 March 31, magnitude threshold $m_t = 5.6$. CMT82-14 is GCMT catalogue for time interval 1982–2014. GEM18-11 is ISC-GEM catalogue (Storchak *et al.* 2015) for time interval 1918–2011, magnitude threshold $m_t = 6.5$; n is the number of events, parameters β and $m_{\rm cm}$ are defined in eq. (2).

March 31 to compare results with Kagan *et al.* (2010, p. 726) and 1982–2014.

Columns 3 and 4 show the β-value estimates. It is assumed that the moment–frequency law follows the G-R relation, either for all moment ranges (Column 3) or at the range from m_t to $m = 7.8$ (Column 4) to exclude the upper part of the distribution. There is practically no difference between the two time periods or between the two columns. This means that the earthquake size distribution is stable in time and there are relatively few large events ($m \geq 7.8$) to significantly influence the β-values estimate. A comparison of these results with table 1 by Kagan *et al.* (2010) demonstrates that the β-values are significantly different for 'fast ridges' only. This can be explained by a low corner magnitude value for these zones ($m_c \simeq 6.8$). The unlimited G-R assumption is clearly violated at the upper tail of the distribution, causing an upwards bias in the β-value evaluation.

The above conclusion is confirmed by the results listed in Column 5, where the $\check{\beta}$-value is determined for the TGR law. In this case the $\check{\beta}$-value for the 'fast ridges' is almost identical to that of table 1 by Kagan *et al.* (2010). The reason for this is that as the size distribution is approximated by the TGR law, both medium-size and large earthquakes are fit by the theoretical curve, using two parameters, β and $m_{\rm cm}$, thus the β-value estimate is not biased by lack of the upper limit for magnitude distribution.

Therefore, perhaps the 'slow-spreading ridges' may have a statistically significant higher β-value, but that could be caused by a mixture of different earthquake populations, each with the same β-value but different m_c values. Our more exhaustive analysis (Bird & Kagan 2004) suggests that the hypothesis of the universality for β-value ($\beta \approx 0.63$) cannot be rejected based on the present data.

The results for the corner magnitude presented in Table 1 are a rather complicated issue. In Columns 6–8, a constant β-value is assumed ($\beta = 2/3$) in order to use appropriate equations from section 3.1.2 of Kagan (2002a). Apparently this assumption causes a strongly biased estimate of $m_{\rm cm}$ for ocean ridges, these values are higher than those of $m_{\rm cg}$ in Column 6. On the other hand, the $m_{\rm cg}$-values for the Gamma distribution are about 0.3 higher than those for $m_{\rm cm}$-values in the upper three rows, as previously found by Kagan (2002a).

Column 8 displays $\tilde{m}_{\rm cm}$-values estimated by using eq. (23) by Kagan & Schoenberg (2001) who proved that usual estimates for the TGR law are biased, especially for the catalogues with a small number of events. They provided a formula to correct the bias (see also Kagan 2002a, eq. 35). The $\tilde{m}_{\rm cm}$-values in Column 8 display the corner magnitude estimate with this correction. Unfortunately, as Kagan & Schoenberg (2001) indicate, as the result of such correction the variance of the estimates increases. The difference between two corner magnitude estimates $\hat{m}_{\rm cm}$ and $\tilde{m}_{\rm cm}$ is not large, so apparently the influence of this bias can be neglected.

Finally, in Column 9 the corner magnitude estimates are reported for the TGR distribution, by determining both $\check{\beta}$ and $\check{m}_{\rm cm}$-values simultaneously (see Column 5). These results compare well with those of table 1 by Kagan *et al.* (2010). Unfortunately, because of the numerical problems (see the last sentence below Table 1) for 1982-2014 we could not evaluate the corner magnitude for the 'Trench' zones; however the m_c-values in Columns 6–8 clearly indicate a significant increase in the corner magnitude value compared to 1982–2008 period. It confirms our result reported in Fig. 3, that $m_{\rm cm} \geq 9.0$ for this period.

In all corner magnitude evaluations in Table 1 we applied statistical techniques developed by Kagan (2002a) to determine the standard error (σ_m) as one value for both the lower and upper limit. This is of course a rough approximation, as Fig. 3 demonstrates; the upper limit often is in effect an infinity. Therefore, to make a more general analysis, in Table 2 we summarize the evaluation of two parameters of the TGR distribution for two periods of the GCMT catalogue and for the ISC-GEM catalogue. These determinations have been made through the analysis of 2-D likelihood maps similar to Fig. 3. The results for CMT82-08/03/31 repeat those in table 1 by Kagan *et al.* (2010); the slight differences between both sets of values are due to the details of the subcatalogues selection.

The results for CMT82-14 generally confirm Table 1 conclusions: the major difference between these two time intervals (1982–2008 and 1982–2014) is the substantial increase in the maximum likelihood $m_{\rm cm}$ value for the 'Trench' zones. With the exception of the higher upper limit for the corner magnitude, which is often equal to infinity, the remaining values of β, $m_{\rm cm}$, and the lower limit for the corner magnitude correspond to that of Table 1. The results for the ISC-GEM catalogue in Table 2 are not that clear, perhaps due to the smaller event numbers and lower accuracy of the catalogue. The values of both TGR parameters display larger standard deviations. Generally these results conform to those of the GCMT catalogue.

3.3 Evaluation of earthquake size distribution parameters using moment conservation principle

Previous evaluations of the moment/frequency distribution parameters in Tables 1 and 2 and Figs 2 and 3 were based on a statistical analysis of earthquake catalogues only. The maximum likelihood

Table 3. Flinn–Engdahl Subduction Seismic Zones, GCMT 1977–2014 December 31, $m_t = 5.8$.

No	FE No	Flinn–Engdahl seismic region name	n	$\beta \pm \sigma_\beta$	$\dot{M}_T$ $\times 10^{27}$	$m_{cg} \pm \sigma_m$	m_o	$\dot{M}_s^o$ $\times 10^{27}$	ψ
1	1	Alaska-Aleutian Arc	307	0.662 ± 0.043	5.096	9.367 ± 0.280	8.0	1.561	0.306
2	5	Mexico-Guatemala	193	0.591 ± 0.051	2.378	9.132 ± 0.284	8.0	1.346	0.566
3	6	Central America	181	0.638 ± 0.054	2.491	9.219 ± 0.285	7.8	0.693	0.278
4	7	Caribbean Loop	63	0.646 ± 0.093	1.048	9.369 ± 0.307	7.4	0.119	0.113
5	8	Andean S. America	344	0.571 ± 0.038	8.493	9.681 ± 0.279	8.8	9.277	1.092
6	12	Kermadec-Tonga-Samoa	485	0.801 ± 0.039	5.945	9.128 ± 0.277	8.1	2.081	0.350
7	13	Fiji Is	86	0.867 ± 0.098	2.293	9.742 ± 0.298	6.8	0.057	0.025
8	14	New Hebrides Is	499	0.595 ± 0.032	4.813	8.939 ± 0.277	8.0	1.955	0.406
9	15	Bismarck-Solomon Is	505	0.593 ± 0.031	4.926	8.947 ± 0.277	8.1	2.459	0.499
10	16	New Guinea	285	0.665 ± 0.045	8.493	9.829 ± 0.281	8.3	1.338	0.158
11	18	Guam-Japan	90	0.854 ± 0.095	2.888	9.888 ± 0.297	7.8	0.303	0.105
12	19	Japan-Kamchatka	560	0.646 ± 0.031	8.493	9.296 ± 0.277	9.2	19.226	2.264
13	20	S.E. Japan-Ryukyu Is	62	0.667 ± 0.096	1.812	9.814 ± 0.307	7.2	0.089	0.049
14	21	Taiwan	115	0.645 ± 0.069	1.529	9.192 ± 0.292	7.7	0.312	0.204
15	22	Philippines	265	0.676 ± 0.047	3.539	9.196 ± 0.281	7.7	0.773	0.219
16	23	Borneo-Celebes	291	0.691 ± 0.045	4.162	9.250 ± 0.280	7.9	1.002	0.241
17	24	Sunda Arc	299	0.661 ± 0.044	6.512	9.582 ± 0.280	8.6	4.187	0.643
18	46	Andaman Is-Sumatra	165	0.731 ± 0.063	2.661	9.345 ± 0.286	9.1	16.848	6.331
		1977–2014 December 31 ZONES	4795	0.657 ± 0.011	77.572	9.347 ± 0.273	9.2	63.626	0.820
		1977–2011 December 31 ZONES	4418	0.658 ± 0.011	77.572	9.347 ± 0.273	9.2	63.568	0.819
		1977–2010 December 31 ZONES	4217	0.654 ± 0.012	77.572	9.361 ± 0.273	9.1	49.074	0.633
		1977–1995 June 30 ZONES	2127	0.633 ± 0.016	77.572	9.420 ± 0.274	8.4	20.670	0.266

Notes: GCMT catalogue, see Ekström *et al.* (2012). FE, Flinn–Engdahl seismic region; n, earthquake number; β, parameter of the power-law distribution of earthquake sizes; m_{cg}, corner magnitude for the Gamma distribution (see eq. 3); $\dot{M}_T$, annual tectonic moment rate, estimated by plate boundaries model (see eq. 10 by Kagan 1997); $\dot{M}_s^o$, empirical annual seismic moment rate calculated by dividing the earthquake scalar moment sum by time; m_o, maximum moment magnitude observed in 1977–2014; $\psi = \dot{M}_s^o / \dot{M}_T$, ratio of seismic to tectonic moment rate. Seismic moment and moment rate are measured in 'dyne cm' and 'dyne cm yr^{-1}', respectively. Tectonic rate $\dot{M}_T$ is calculated using Bird & Kagan (2004) parameters: seismogenic width $W = 104$ km, elastic shear modulus $\mu = 49$ GPa, and seismic coupling coefficient $\chi = 0.5$.

evaluations of the parameters for tectonic zones (Fig. 1) supply important information of their possible values that can be used in GEAR1 forecasts. However, for almost all zones the upper limit of magnitude distribution cannot be obtained with the presently available data: in Table 2 the limits are shown as infinite.

Zöller & Holschneider (2016) use a truncated G-R law with the maximum possible magnitude called m_{max}. They also argue that modern earthquake catalogues are insufficient for reliable evaluation of m_{max} by standard statistical techniques, and they suggest that an alternative method to evaluate m_{max} is through comparison of tectonic loading rate to seismic rate.

3.3.1 Method

As Kagan & Jackson (2013) indicate, m_c can best be evaluated by comparing the seismic moment rate with the tectonic rate using the moment conservation principle: the seismic rate should be equal or smaller than the tectonic rate. Quantitative plate tectonics and space geodetic methods currently provide a numerical estimate of the tectonic deformation rate ($\dot{M}_T$) for all major tectonic plate boundaries and continental regions of significant distributed deformation (Kagan 1997; Bird & Kagan 2004; Kagan *et al.* 2010; Bird & Kreemer 2015).

Table 3 lists the evaluation of β and m_{cg} parameters for the Flinn–Engdahl (FE; Gutenberg & Richter 1954, fig. 1; Flinn *et al.* 1974; Young *et al.* 1996) zones listed in the sequential order. These FE regions correspond to major subduction zones. They have been selected because the FE regionalization had been defined before the GCMT catalogue started, thus eliminating a selection bias.

The GCMT catalogue 1977–2014 in different temporal subdivisions is used. We calculate empirical annual seismic moment rate $\dot{M}_s^o$ by dividing the earthquake scalar moment sum by time. High variation of $\dot{M}_s^o$ is to be expected; as Zaliapin *et al.* (2005) show, the sum of power-law distributed variables exhibits high degree of fluctuation and converges very slowly to a limiting distribution. The ratio $\psi = \dot{M}_s^o / \dot{M}_T$ of the empirical seismic to tectonic moment rate depends strongly on the maximum observed earthquake (m_o): it exceeds 1.0 for those FE regions where $\sim m9$ occurred during 1977–2014 period, whereas in the other regions the ψ-values are significantly smaller.

The corner magnitude values m_{cg} are computed by comparing the tectonic and seismic moment rates, the latter one in its turn depends on earthquake number rate (eq. 6). Details of calculations are provided by Kagan (2002b) and Kagan & Jackson (2013). From the analysis of the parameter values for 18 major subduction zones a conclusion can be drawn that both parameters (β and m_{cg}) are practically the same for all these zones.

The lower four lines in the table supply total parameter values for all 18 FE zones, estimated for four different time periods. Whereas the event number (n), the maximum observed earthquake magnitude (m_o), the empirical annual seismic moment rate ($\dot{M}_s^o$), and the ratio of the seismic to tectonic moment rate ψ change significantly over the duration of the catalogue, the estimated corner magnitude remains the same ($m_{cg} \simeq 9.3$). This testifies that the

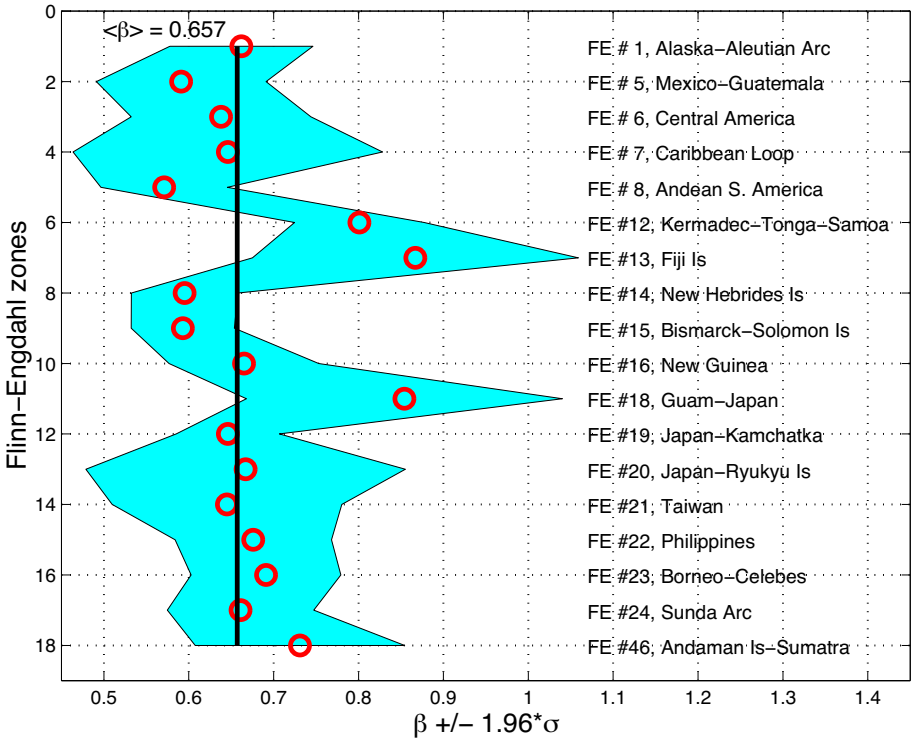

Figure 4. Parameter β distribution in the Flinn–Engdahl (FE) subduction zones Flinn–Engdahl; average β-values are shown by circles. GCMT catalogue 1977–2014 December 31. The ordinate numbers are sequential numbers of subduction zones considered, the FE numbers and names for these zones are shown in the right-hand part of the diagram. Average region's β and ± 1.96 standard deviations are shown by shaded zones, these zones correspond to 95 per cent confidence limits. The solid line corresponds to the average $\langle\beta\rangle = 0.657$ for all subduction zones.

moment conservation principle yields a consistent estimate of the corner magnitude.

3.3.2 *Results*

In the next few diagrams the results for the FE zones are displayed in more detail. Fig. 4 shows the β-values determined for 18 FE zones listed in a sequential order. Similar plots have been constructed by Kagan (1997) and Kagan & Jackson (2013). The diagram again demonstrates that (1) the β-values do not depend significantly on the catalogue duration, though their standard errors decrease as the duration and earthquake numbers increase; (2) the β-values are approximately the same for all the zones, and the hypothesis of the values equality cannot be statistically rejected with 95 per cent confidence (Kagan 1997, pp. 2843–2844). The additional data since 1995 makes the argument for a common β stronger.

Fig. 5 shows the distribution of the corner magnitude obtained, using eq. (6), for the GCMT earthquake catalogue. The tectonic rate for the 1977–2014 December 31 period is calculated by using Bird & Kagan (2004) parameters: $W = 104$ km, $\mu = 49$ GPa; for simplicity we use $\chi = 0.5$ instead of $\chi = 0.69$. Estimates of m_{cg} for all diagrams in all the subduction zones are statistically indistinguishable. Thus all such zones may have the same corner magnitude. Some parameters may vary between individual zones, but the results are consistent with the hypothesis that the product $\mu \times \chi \times W$, which enters the tectonic moment equation, is nearly the same for all zones.

In Fig. 6, we repeat m_{cg} determination for the ISC-GEM catalogue 1918–2011. There is little difference between the results of Figs 5 and 6.

Fig. 7 again demonstrates how the catalogue duration affects the ratio of the seismic rate to the tectonic rate for different subduction zones. This ratio is below 1.0 for a shorter catalogue, but it increases to a value close to 1.0 for a longer list. This increase is caused mainly by a few large earthquakes that struck South America, Sumatra and Japan regions.

4 EARTHQUAKE NUMBER DISTRIBUTION

A quantitative earthquake forecast requires estimating the earthquake number distribution (Schorlemmer & Gerstenberger, 2007; Zechar *et al.* 2013). A common assumption, as used in the CSEP tests, is that the numbers are described by the Poisson distribution. However it is clear that the Poisson assumption for the earthquake number distribution is incorrect, especially for the catalogues with a lower magnitude threshold. For instance, Michael (2011, fig. 3) found that the global catalogue violated the Poisson model at the threshold values of $m7.5$ and below; Shearer & Stark (2012, table 1) found this for $m7$ and below.

One conventional way to treat this problem is to decluster an earthquake catalogue (Schorlemmer *et al.* 2007). But there are several declustering procedures, mostly based on *ad-hoc* rules. Therefore, it is important to derive and investigate earthquake number distribution in real earthquake catalogues.

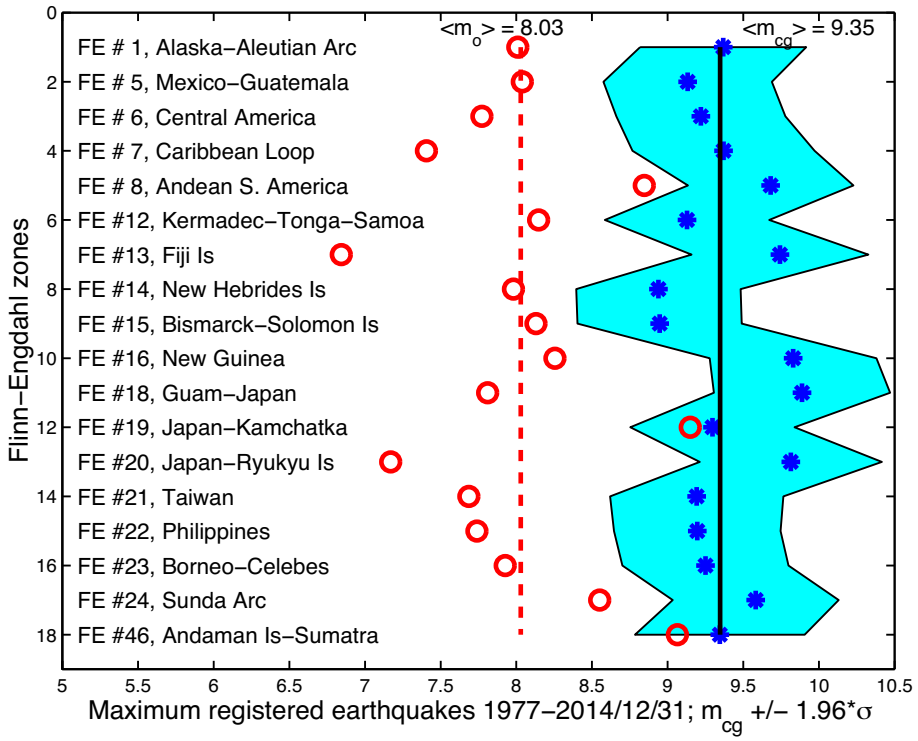

Figure 5. GCMT catalogue 1977–2014. The corner moment magnitude m_{cg} distribution (see eq. 3) in the Flinn–Engdahl subduction zones. Average region's m_{cg} (blue disks) and ± 1.96 standard deviations are shown by shaded zones, these zones correspond to 95 per cent confidence limits. The solid line corresponds to the average $\langle m_{cg} \rangle = 9.35$ for all subduction zones. In m_{cg} calculations we use the parameters of the tectonic motion as proposed by Bird & Kagan (2004): $W = 104$ km, $\mu = 49$ GPa, $\chi = 0.5$. Red circles show events with the maximum magnitude m_o in the regions during the catalogue time interval. The dashed line corresponds to the average $\langle m_o \rangle = 8.03$ for all subduction zones.

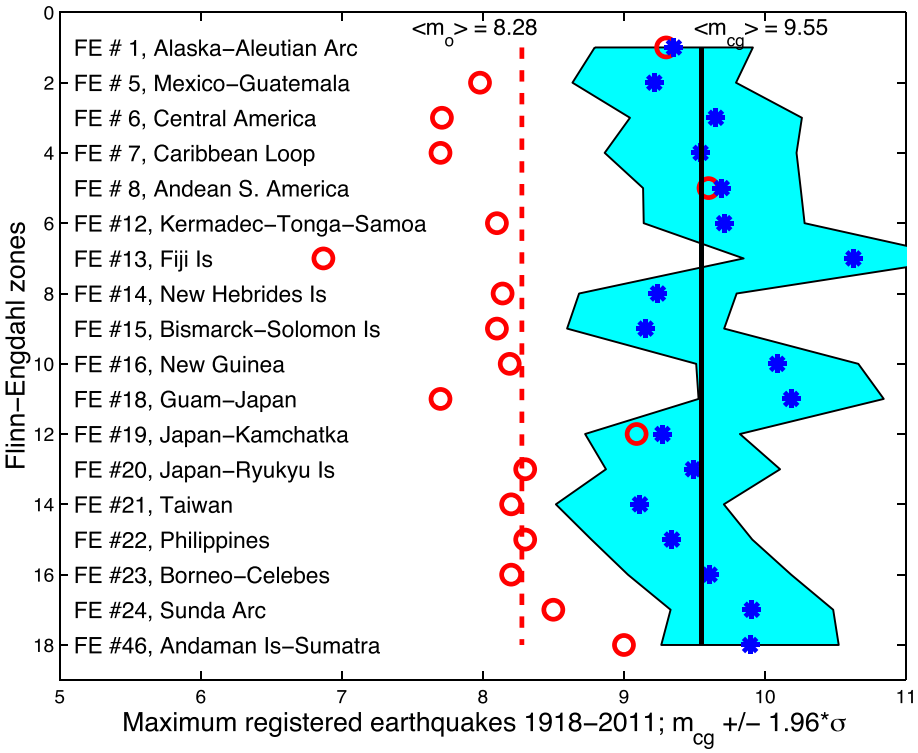

Figure 6. ISC-GEM catalogue 1918–2011 (Storchak *et al.* 2015) is used. The corner moment magnitude m_{cg} distribution (see eq. 3) in the Flinn–Engdahl subduction zones. The solid line corresponds to the average $\langle m_{cg} \rangle = 9.55$ for all subduction zones. In m_{cg} calculations, we use the parameters of the tectonic motion as proposed by Bird & Kagan (2004): $W = 104$ km, $\mu = 49$ GPa, $\chi = 0.5$. Circles show events with the maximum magnitude m_o in the regions during the catalogue time interval. The dashed line corresponds to the average $\langle m_o \rangle = 8.28$ for all subduction zones.

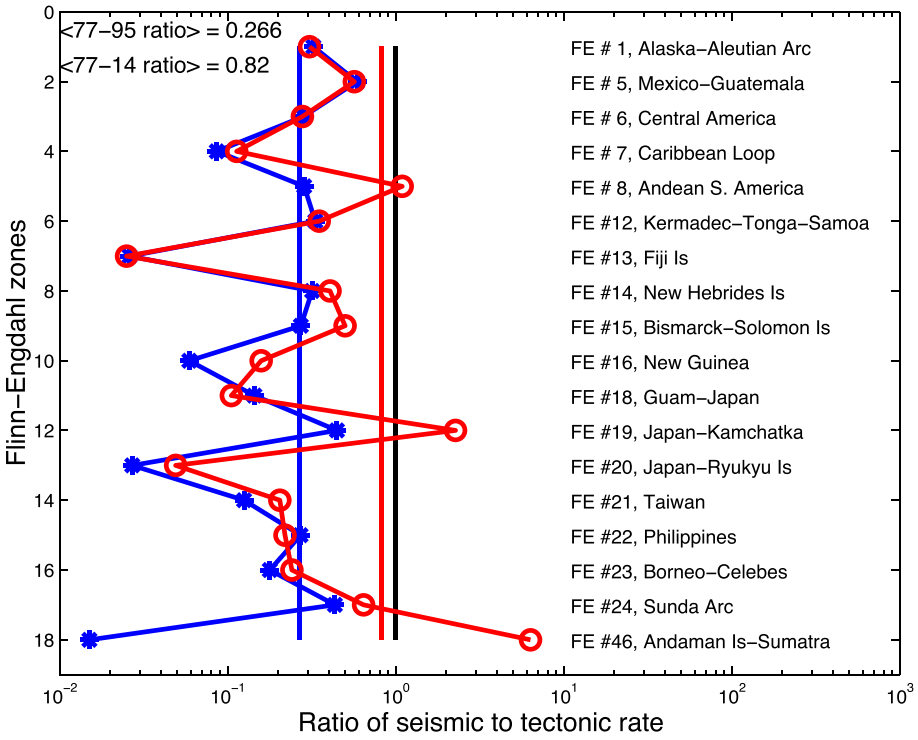

Figure 7. Ratio ψ of the empirical seismic to tectonic rate ($\psi = \dot{M}_s^o/\dot{M}_T$) in the Flinn–Engdahl subduction zones for the GCMT catalogue 1977–1995 June 30 (blue lines) and 1977–2014 (red lines). Vertical lines show the average ratio for all regions ($\psi_1 = 0.266$; $\psi_2 = 0.82$); the black line corresponds to the ratio of 1.0. See also the last column of Table 3.

4.1 Method and theoretical number distributions

In contrast to the one-parameter Poisson distribution widely used to describe earthquake occurrence, the NBD has two parameters (Kozubowski & Podgórski 2009; Kagan 2010; Harte 2015). The second parameter can be used to characterize the clustering or overdispersion of a process.

Fig. 8 displays annual earthquake numbers for the PDE catalogue (see also fig. 5 by Kagan & Jackson 2000 or fig. 5 by Kagan 2010). Even a casual inspection suggests that the numbers are overdispersed compared to the Poisson process: the standard deviation is larger than the square root of the average as expected in the Poisson process. The number peaks can usually be traced back to strong main shocks with extensive aftershock sequences.

Jackson & Kagan (1999, fig. 3) as well as Kagan & Jackson (2011, figs 3 and 4) showed that the Poisson law is not a good approximation of the number distribution, whereas NBD provides a good fit. Kagan (2010) derived NBD theoretically as a consequence of the branching structure of the earthquake process. His tables 1–3 display three dependencies of the NBD parameter estimates: (1) on the magnitude threshold (m_t); (2) on the time intervals (ΔT) a catalogue time-span is subdivided; and (3) on a subdivision of a catalogue space window. Three parametrizations of the NBD are applied in these tables.

In this paper we apply the number distributions for testing earthquake forecasts. The standard NBD form (Kagan 2010, eqs 15–17) is most appropriate for this purpose. In this parametrization the NBD clustering feature is characterized by the parameter θ ($0.0 \le \theta \le 1.0$). If $\theta \to 1.0$ the process approaches the Poisson distribution. A sum of two statistically independent NBD variables with the same value of θ, but parameters τ_1 and τ_2 is also NBD variable with same θ and $\tau = \tau_1 + \tau_2$. Thus, in our case in some sense θ indicates the degree of clustering, and τ shows the earthquake population size.

To test the GEAR1 forecast we calculate the Poisson cumulative distribution by using the following formula for the survivor function (Kagan & Jackson 2011)

$$1-F(k) = P(N < k) = \frac{1}{k!}\int_{\lambda}^{\infty} y^k\, e^{-y}\, \mathrm{d}y \;=\; 1-\Gamma(k+1,\,\lambda), \tag{7}$$

where $F(k)$ is the cumulative distribution function, λ is the event rate of occurrence, and $\Gamma(k+1,\,\lambda)$ is an incomplete gamma function.

The NBD probability density is defined as (Kagan 2010)

$$f\,(k) \;=\; \binom{\tau+k-1}{k} \;\times\; \theta^{\tau}(1-\theta)^k\,, \tag{8}$$

where $k = 0, 1, 2, \ldots$. The parameters have limits of $0 \le \theta \le 1$, and $\tau > 0$. The NBD survivor distribution function is calculated using (Kagan & Jackson 2011)

$$1-F(k) = P(N < k) = \frac{1}{B(\tau,\,k+1)}\int_{0}^{\theta} y^{\tau-1}\,(1-y)^k\,\mathrm{d}y, \tag{9}$$

where $B(\tau,\,k+1)$ is the beta function. The right-hand part of the equation corresponds to the incomplete beta function, $B(\tau,\,k+1,\,x)$ (Gradshteyn & Ryzhik 1980).

The ratio of the process variance (V_2) to its rate ($V_1 = \lambda$) is

$$V_2 \;=\; \frac{V_1}{\theta}, \tag{10}$$

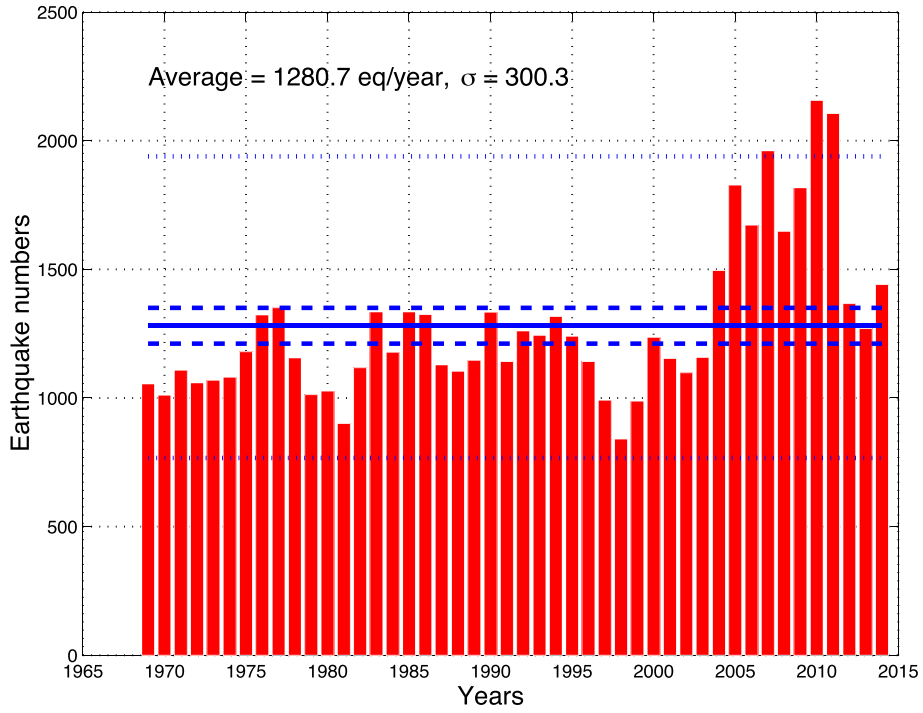

Figure 8. Annual numbers of earthquakes $m \geq 5.0$ in the global PDE catalogue, 1969–2014. Blue horizontal line shows average annual earthquake number, two blue lines demonstrate 95 per cent confidence areas for the Poisson (dashed lines) and NBD (dotted lines) distributions. Only three annual earthquake numbers are outside of the NBD confidence intervals. For 95 per cent confidence one should expect that about 5 per cent of 46 entries would exceed the limits.

that is, for small θ the process is over-dispersed, whereas if $\theta = 1$ the ratio is also equal to 1.0 as it should for the Poisson law.

4.2 Results

In this work, we recalculate the parameter values for the PDE catalogue of 1969–2014, providing more extensive results for the five global tectonic zones (Fig. 1) that are used in the GEAR1 forecast. In Table 4, we list the parameter values of earthquake number distributions in the same format as tables 1–3 by Kagan (2010). We also list the Poisson and the NBD parameters for annual numbers in the global PDE catalogue as well as in five tectonic zones.

The constraint that θ is located between zero and one means that the NBD distribution describes a range of behaviours from very strong clustering (θ near zero) to essentially Poissonian (θ near one). The distribution has no validity for θ greater than one. However, the procedure for estimating θ may give values greater than one, especially when the number of events per time interval is very low. Hence in Table 4, we report parameters only for subcatalogues for which the threshold magnitude was low enough that the estimated θ values did not exceed one.

Table 4 reveals that the estimated θ value increases with increasing threshold magnitude in each tectonic category. By extrapolation we see that θ reaches 1.0 at a threshold magnitude of about 7.8 to 8.0, similar to that estimated by Kagan (2010). We conclude that the Poisson assumption is adequate for earthquakes above magnitude 7.0. Table 4 shows results for the PDE catalogue; parameters for the GCMT catalogue, not shown, give similar results.

Comparing Table 4 with table 1 by Kagan (2010) shows that the θ-values are generally lower for the updated 1969–2014 catalogue. This may be caused by a series of very large earthquakes which occurred in 2008–2014 (see Fig. 8). These earthquakes were accompanied by extensive aftershock sequences, increasing the catalogue clustering property. In catalogue subdivisions with the threshold $m_t \geq 6.5$, the number distribution is close to the Poisson one, since the θ-parameter approaches 1.0. Therefore, the usual Poisson assumption for the number distribution should not cause significant errors. However, if one is interested in the forecast of smaller earthquakes, the Poisson law must be replaced by the NBD in the forecast tests. GEAR1 program (Bird *et al.* 2015) forecasts earthquakes in the magnitude range from 6.0 to 9.0 in steps of 0.1. Therefore, a forecast for the first magnitude bins would require application of the NBD for the number tests.

In Fig. 9, we display the fit of a cumulative distribution for annual earthquake numbers in the PDE catalogue. The difference between the Poisson and NBD distributions is very large in this plot, because of a lower magnitude threshold in the PDE catalogue. Since $\theta = 0.0145$ for this earthquake set, the variance of the annual number distribution should be about 69 times higher than that for the Poisson law (see eq. 10) for which the variance is equal to the rate ($\lambda = 1280.7$). Therefore in the diagram the Poisson curve has the standard deviation $\sigma \approx 35.8 = \sqrt{\lambda}$, whereas for the NBD $\sigma \approx 300.3$ (see Fig. 8). Parameters for the NBD are calculated using eqs (16) and (17) in Kagan (2010).

The 95 per cent confidence area is symmetric around the average for the Poisson curve (the limits are from 1211.1 to 1350.0). This happens because for large λ-values the Poisson distribution can be closely approximated by the Gaussian one. On the other hand, the NBD curve shows asymmetry: from the middle λ-point the confidence area is more extended to the right than to the left (95 per cent confidence limits are from 766.7 to 1938.9).

Table 4. Values of NBD parameters for various subdivisions of the 1969–2014 PDE catalogue.

	m_t	n	N	λ	α	a	θ	τ	ΔT
1	2	3	4	5	6	7	8	9	10
G	7.0	560	46	12.2	0.0130	0.1582	0.8634	76.94	365.2
G	6.5	1636	46	35.6	0.0181	0.6426	0.6088	55.35	365.2
G	6.0	4827	46	104.9	0.0384	4.0265	0.1989	26.06	365.2
G	5.5	16653	46	362.0	0.0459	16.600	0.0568	21.81	365.2
G	5.0	58914	46	1280.7	0.0530	67.886	0.0145	18.87	365.2
0	5.5	637	46	13.8	0.0400	0.5541	0.6435	24.99	365.2
0	5.0	2609	46	56.7	0.1472	8.3512	0.1069	6.79	365.2
1	7.0	116	46	2.52	0.2307	0.5817	0.6322	4.34	365.2
1	6.5	312	46	6.78	0.1351	0.9161	0.5219	7.40	365.2
1	6.0	798	46	17.3	0.0571	0.9905	0.5024	17.51	365.2
1	5.5	2578	46	56.0	0.0599	3.355	0.2296	16.70	365.2
1	5.0	9340	46	203.0	0.0635	12.89	0.0720	15.76	365.2
2	6.0	256	46	5.57	0.0416	0.2317	0.8119	24.02	365.2
2	5.5	1062	46	23.1	0.1090	2.516	0.2844	9.18	365.2
2	5.0	4445	46	96.6	0.1086	10.50	0.0870	9.21	365.2
3	6.5	63	46	1.37	0.0663	0.0908	0.9168	15.09	365.2
3	6.0	359	46	7.8	0.0301	0.2346	0.8099	33.26	365.2
3	5.5	1372	46	29.8	0.1324	3.949	0.2020	7.55	365.2
3	5.0	3983	46	86.6	0.1814	15.71	0.0598	5.51	365.2
4	7.0	405	46	8.8	0.0337	0.2969	0.7711	29.66	365.2
4	6.5	1145	46	24.9	0.0272	0.6773	0.5962	36.75	365.2
4	6.0	3244	46	70.5	0.0663	4.676	0.1762	15.08	365.2
4	5.5	11004	46	239.2	0.0608	14.54	0.0644	16.46	365.2
4	5.0	38537	46	837.8	0.0648	54.26	0.0181	15.44	365.2

Notes: In Column 1: G means that the global catalogue is used; 0, plate interior; 1, Active continent; 2, Slow ridge; 3, Fast ridge; 4, Trench (subduction zones), see Kagan *et al.* (2010) and Fig. 1. m_t is the magnitude threshold, N is the number of time intervals, ΔT is the interval duration in days; for parameters of NBD: λ, α, a, θ and τ see Kagan (2010), for θ and τ see also eq. (8).

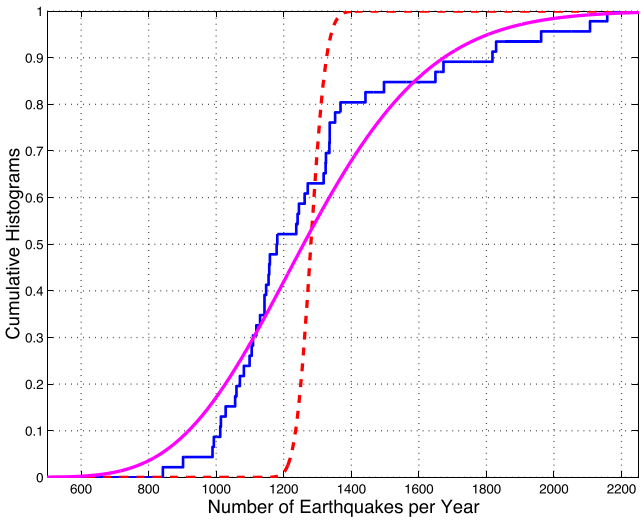

Figure 9. Cumulative distribution of yearly earthquake numbers for the global PDE catalogue, 1969–2014, $m \geq 5.0$. The step function shows the observed distribution, the dashed curve is the theoretical Poisson distribution for $\lambda = 1280.7$ (see Table 4 and eq. 7) and the solid curve is the fitted negative-binomial curve for $\theta = 0.0145$ and $\tau = 18.87$ (Table 4 and eq. 9). The negative-binomial curve has a better fit than the Poisson curve.

5 CONCLUSIONS

In this paper we address two problems connected with extensions of the GEAR1 forecast (Bird *et al.* 2015): (1) updating the moment/frequency relation using newly available catalogue information and applying more refined methods to evaluate the corner magnitude (m_c) values; (2) preparing appropriate methods to adequately carry out the number test, that is, to calculate the significance limit of the future earthquake activity levels.

5.1 Magnitude distribution

The GEAR1 program uses the corner magnitude values for five tectonic zones (Fig. 1) specified by Kagan *et al.* (2010), employing a complicated method to infer activity rates for magnitude ranges 6.0–9.0. For the 'Tectonic' forecast (Bird & Kreemer 2015, pp. 157–158), the authors try several versions of cell smoothing, adjustment and re-normalizing to obtain a final forecast variant appropriate for the relevant magnitude range. Similarly, another method based on elaborate smoothing seismicity was employed for the 'Seismicity' forecast by Kagan & Jackson (2000, 2011) and by Bird *et al.* (2015). This forecast was combined with the Tectonic model to obtain a 'Hybrid' forecast, which is presented to CSEP for prospective testing.

In Section 3, we use two methods to update the moment/frequency relation parameters: statistical techniques that analyse earthquake catalogues alone by likelihood methods, and the moment conservation principle that equates seismic moment rate with tectonic moment rate inferred from geodesy and geology. The former method is well studied, but it fails to provide an upper limit on the corner magnitude without vastly more data than presently available. Generally, the new results are consistent with past estimates (e.g. Tables 1 and 2), but the corner magnitude estimates tend to increase

with time, as earthquake magnitude records are broken. Even with these new techniques, the true upper limits to earthquake size are not well constrained with available data.

The moment conservation principle allows us to evaluate the upper limit of the corner magnitude under several assumptions. We must assume that the current seismic moment rate is equal to the long-term tectonic rate, and that physical parameters describing plate-boundary geometry, coupling, and rheology are known. Table 3 lists estimates of corner magnitude for the major subduction zones and for the sum of the zones. Although all the m_{cg} values are within a narrow range (8.9–9.6), the absolute level of these values depends on the parameters of the tectonic rate calculation.

5.2 Number distribution

To investigate the earthquake number distributions following our previous effort (Kagan 2010), we calculated parameter estimates for two traditional integer-valued distributions: Poisson and negative binomial (see Table 4). Fig. 9 displays the fit of these distributions to annual earthquake numbers in the PDE catalogue. In Table 4, we calculated the parameters for the annual rates only. These are the annual rates most frequently tested by CSEP. Tables 1–3 by Kagan (2010) list the rates for the other time periods and various earthquake catalogues. The Poisson distribution is clearly inadequate to describe the global annual numbers of magnitude 6.5 and smaller earthquakes. The observed rates are much more diverse, relative to their means, because of temporal clustering, which is much better described by the NBD. For earthquakes larger than magnitude 6.5, the Poisson distribution works reasonably well.

ACKNOWLEDGEMENTS

We are grateful to Peter Bird of UCLA for useful discussions. The authors appreciate partial support from the National Science Foundation through grant EAR-1045876, as well as from the Southern California Earthquake Center (SCEC). SCEC is funded by NSF Cooperative Agreement EAR-0529922 and USGS Cooperative Agreement 07HQAG0008. The comments by Dr A. J. Michael and by an anonymous reviewer as well as by the Associate Editor Dr Saskia Goes have significantly improved the presentation. Publication 6228, SCEC.

REFERENCES

Bateman, H. & Erdelyi, A., 1953. *Higher Transcendental Functions,* McGraw-Hill Co.

Bird, P., 2003. An updated digital model of plate boundaries, *Geochem. Geophys. Geosyst.,* **4**(3), 1027, doi:10.1029/2001GC000252.

Bird, P. & Kagan, Y.Y., 2004. Plate-tectonic analysis of shallow seismicity: apparent boundary width, beta, corner magnitude, coupled lithosphere thickness, and coupling in seven tectonic settings, *Bull. seism. Soc. Am.,* **94**(6), 2380–2399 (plus electronic supplement).

Bird, P. & Kreemer, C., 2015. Revised tectonic forecast of global shallow seismicity based on version 2.1 of the Global Strain Rate Map, *Bull. seism. Soc. Am.,* **105**(1), 152–166 (plus electronic supplement).

Bird, P., Jackson, D.D., Kagan, Y.Y., Kreemer, C. & Stein, R.S., 2015. GEAR1: a Global Earthquake Activity Rate model constructed from geodetic strain rates and smoothed seismicity, *Bull. seism. Soc. Am.,* **105**(5), 2538–2554 (plus electronic supplement).

Di Giacomo, D., Bondar, I., Storchak, D.A., Engdahl, E.R., Bormann, P. & Harris, J., 2015. ISC-GEM: Global Instrumental Earthquake Catalogue (1900–2009), III. Re-computed M_S and m_b, proxy M_W, final magnitude composition and completeness assessment, *Phys. Earth planet. Inter.,* **239**(2), 33–47.

Ekström, G., Nettles, M. & Dziewonski, A.M., 2012. The global CMT project 2004–2010: centroid-moment tensors for 13,017 earthquakes, *Phys. Earth planet. Inter.,* **200–201,** 1–9.

Flinn, E.A., Engdahl, E.R. & Hill, A.R., 1974. Seismic and geographical regionalization, *Bull. seism. Soc. Am.,* **64,** 771–992.

Gradshteyn, I.S. & Ryzhik, I.M., 1980. *Table of Integrals, Series, and Products,* Academic Press, 1160 pp.

Gutenberg, B. & Richter, C.F., 1954. *Seismicity of the Earth and Associated Phenomena,* Princeton Univ. Press, 310 pp.

Hanks, T.C., 1992. Small earthquakes, tectonic forces, *Science,* **256,** 1430–1432.

Harte, D.S., 2015. Log-likelihood of earthquake models: evaluation of models and forecasts, *Geophys. J. Int.,* **201**(1), 711–723.

Jackson, D.D. & Kagan, Y.Y., 1999. Testable earthquake forecasts for 1999, *Seismol. Res. Lett.,* **70**(4), 393–403 (with electronic supplement).

Kagan, Y.Y., 1997. Seismic moment-frequency relation for shallow earthquakes: regional comparison, *J. geophys. Res.,* **102**(B2), 2835–2852.

Kagan, Y.Y., 2002a. Seismic moment distribution revisited: I. Statistical results, *Geophys. J. Int.,* **148**(3), 520–541.

Kagan, Y.Y., 2002b. Seismic moment distribution revisited: II. Moment conservation principle, *Geophys. J. Int.,* **149**(3), 731–754.

Kagan, Y.Y., 2003. Accuracy of modern global earthquake catalogs, *Phys. Earth planet. Inter.,* **135**(2–3), 173–209.

Kagan, Y.Y., 2010. Statistical distributions of earthquake numbers: consequence of branching process, *Geophys. J. Int.,* **180**(3), 1313–1328.

Kagan, Y.Y. & Jackson, D.D., 2000. Probabilistic forecasting of earthquakes, *Geophys. J. Int.,* **143**(2), 438–453.

Kagan, Y.Y. & Jackson, D.D., 2011. Global earthquake forecasts, *Geophys. J. Int.,* **184**(2), 759–776.

Kagan, Y.Y. & Jackson, D.D., 2013. Tohoku earthquake: a surprise?, *Bull. seism. Soc. Am.,* **103**(2B), 1181–1194.

Kagan, Y.Y. & Schoenberg, F., 2001. Estimation of the upper cutoff parameter for the tapered Pareto distribution, *J. Appl. Probab.,* **38A,** 158–175.

Kagan, Y.Y., Bird, P. & Jackson, D.D., 2010. Earthquake patterns in diverse tectonic zones of the Globe, *Pure appl. Geophys.,* **167**(6/7), 721–741.

Kozubowski, T.J. & Podgórski, K., 2009. Distributional properties of the negative binomial Lévy process, *Probab. Math. Stat.,* **29**(1), 43–71.

Kreemer, C., Blewitt, G. & Klein, E.C., 2014. A geodetic plate motion and Global Strain Rate Model, *Geochem. Geophys. Geosyst.,* **15,** 3849–3889.

Meerschaert, M.M., Roy, P. & Shao, Q., 2012. Parameter estimation for exponentially tempered power law distributions, *Commun. Stat. - Theory Methods,* **41,** 1839–1856.

Michael, A.J., 2011. Random variability explains apparent global clustering of large earthquakes, *Geophys. Res. Lett.,* **38,** L21301, doi:10.1029/2011GL049443.

Michael, A.J., 2014. How complete is the ISC-GEM Global Earthquake Catalog?, *Bull. seism. Soc. Am.,* **104**(4), 1829–1837.

Schorlemmer, D. & Gerstenberger, M.C., 2007. RELM testing Center, *Seismol. Res. Lett.,* **78**(1), 30–35.

Schorlemmer, D., Gerstenberger, M.C., Wiemer, S., Jackson, D.D. & Rhoades, D.A., 2007. Earthquake likelihood model testing, *Seismol. Res. Lett.,* **78**(1), 17–29.

Shearer, P. & Stark, P.B., 2012. Global risk of big earthquakes has not recently increased, *Proc. Natl. Acad. Sci. USA,* **109**(3), 717–721.

Storchak, D.A., Di Giacomo, D., Engdahl, E.R., Harris, J., Bondar, I., Lee, W.H., Bormann, K.P. & Villaseqor, A., 2015. The ISC-GEM Global Instrumental Earthquake Catalogue (1900–2009): Introduction, *Phys. Earth planet. Inter.,* **239,** 48–63.

U.S. Geological Survey, 2008. *Preliminary Determinations of Epicenters (PDE),* 2008.

Young, J.B., Presgrave, B.W., Aichele, H., Wiens, D.A. & Flinn, E.A., 1996. The Flinn-Engdahl regionalisation scheme: the 1995 revision, *Phys. Earth planet. Inter.,* **96,** 223–297.

Zaliapin, I.V., Kagan, Y.Y. & Schoenberg, F.P., 2005. Approximating the distribution of Pareto sums, *Pure appl. Geophys.,* **162**(6–7), 1187–1228.

Zechar, J.D., Schorlemmer, D., Werner, M.J., Gerstenberger, M.C., Rhoades, D.A. & Jordan, T.H., 2013. Regional earthquake likelihood models. I: First-order results, *Bull. seism. Soc. Am.,* **103**(2a), 787–798.

Zöller, G. & Holschneider, M., 2016. The earthquake history in a fault zone tells us almost nothing about $m_{\max}$, *Seismol. Res. Lett.,* **87**(1), 132–137.